Electrochimica Acta 182 (2015) 272–279

Contents lists available at ScienceDirect

Electrochimica Acta

journal homepage: www.elsevier.com/locate/electacta

Cu particles decorated pomegranate-structured SnO_2@C composites as anode for lithium ion batteries with enhanced performance

WeiWei Wen[a], Mingzhong Zou[a], Qian Feng[a], Jiaxin Li[a,b,*], Lunhui Guan[b], Heng Lai[a], Zhigao Huang[a,*]

[a] College of Physics and Energy, Fujian Normal University, and Fujian Provincial Key Laboratory of Quantum Manipulation and New Energy Materials, Fuzhou, 350007, China

[b] Fujian Institute of Research on the Structure of Matter, Chinese Academy of Sciences, Fuzhou 350002, China

ARTICLE INFO

Article history:
Received 10 June 2015
Received in revised form 13 August 2015
Accepted 15 September 2015
Available online 21 September 2015

Keywords:
Lithium ion batteries
Pomegranate-structured materials
SnO_2@C/Cu anodes
Electrochemical performance

ABSTRACT

In this paper, homogeneous composites of pomegranate-structured SnO_2@C/Cu have been prepared by a simple hydrothermal reaction coupled with wet-chemical reduction, and directly used as anode materials for lithium ion batteries (LIBs). These SnO_2@C/Cu anodes with an unique architecture show good LIB performance with a capacity of 660 mAh g^{-1} tested at 600 mA g^{-1} after 50 cycles and good rate performance at room temperature. Compared with the pure SnO_2 and SnO_2@C, SnO_2@C/Cu anodes exhibit much better low-temperature electrochemical performance including reversible capacity, cycling performance, and rate performance. The good LIB performance of SnO_2@C/Cu anodes should be associated with carbon shell and the conducting Cu particles. This unique configuration can prevent the agglomeration of active materials and facilitate electron conduction especially at a relative low temperature, and obtain the capacity stability in cycling process for LIBs.

1. Introduction

Increasing energy demands have stimulated extensive research on alternative anode materials for lithium ion batteries (LIBs). As a promising eco-friendly energy storage material, SnO_2 has attracted great attention due to its high theoretical energy storage capacity [1–4]. However, the poor electrochemical activity and large volume variation of more than 250% during the course of lithium intercalation or release, hamper their potential practical usage in LIBs [3–4]. Moreover, SnO_2 as a kind of semiconductor would present an increasing electric resistance with decreasing temperature. Usually, the conductivity attenuation combined with substantial microstructure change at low temperature, resulting in large interface polarization and performance deterioration, hampers their high-level applications in LIBs [5]. Therefore, it is still urgent to design related strategies to enhance the electrochemical performance of SnO_2-based anodes especially at low temperature.

Up to now, many useful strategies have been proposed to overcome these issues. For instance, the preparation of nanostructured SnO_2-based materials [6–12], such as spheres, nanowires, nanotubes, nanoflakes and nanoplatelets has been investigated for shortening Li^+ diffusion length and accommodating large mechanical strain associated with structure and volume changes. Researchers also focused on using varied carbonaceous materials including carbon nanotubes, carbon layer and graphene as buffer carriers for suppressing the pulverization and capacity fading of SnO_2-based anodes [13–16]. It is noted that various nanostructures can only give a limited improvement on the electrochemical performance of SnO_2-based anodes generally at low test rates. Meanwhile, for the SnO_2 composites coupled with carbonaceous materials, the connection between SnO_2 and carbonaceous materials is usually weak, which still lead to large volume change during cycling process [17]. Besides, for improving the low temperature performance, enormous efforts have been devoted to mitigate the detrimental effects of conductivity attenuation, including the utilization of metal nanoparticles attached on the surface of anode materials and the utilization of metal layer covered on the materials. *Huang et al.* [18] reported that the anode of Fe_2O_3 carbon nanofibers can exhibit an obvious enhanced low-temperature electrochemical performance by Ag incorporation. It is believed that the Ag particles possess better conductivity at low temperature than that at room temperature, thereby significantly improving their electrochemical performance at low temperature. Recently, for the price consideration, a cheap

* Corresponding authors. Telephone/Fax: 86 591 22867577.
E-mail addresses: ljx@fjirsm.ac.cn, ljx3012982@yahoo.com (J. Li), zghuang@fjnu.edu.cn (Z. Huang).

http://dx.doi.org/10.1016/j.electacta.2015.09.082
0013-4686/

reliable metal of Fe also with good electrical conductivity has been used instead of Ag nanoparticles for enhancing the low-temperature performance for LIBs [5]. To a certain extent, the electrochemical performance for SnO_2 anode materials can be slightly improved by each of above-mentioned strategies. Nevertheless, for SnO_2 anode materials, the hypothesis that how to develop an effective method to simultaneously integrate those three strategies and further to fabricate anode composites with highly dispersed cheap metal nanoparticles and excellent conductivity, and further achieve excellent low temperature electrochemical performance is highly desired. In this study, this hypothesis has been carried out.

More importantly, the recent report revealed that the Si-based anodes with pomegranate-like structure can tackle the main challenges associated with structural degradation and instability caused by the large volume change for LIBs [19]. Similarly, *Fang* et al [20]. reported that a homogeneous composite of SnO_2 anodes, where 3–9 nm SnO_2 nanoparticles are embedded in about 50 nm diameter primary carbon nanospheres, can exhibit a high capability and excellent cycling and rate performance, holding great potential as a high-rate and stable anode material for lithium storage. Here, our design is inspired by the structure of a pomegranate and above reports. Cu particles decorated pomegranate-structured SnO_2@C (denoted as SnO_2@C/Cu) composites as anode materials for LIBs have been prepared by a simple hydrothermal reaction coupled with wet-chemical reduction. These SnO_2@C/Cu anodes provided with the unique architectures exhibit outstanding lithium battery performance with a capacity of 660 mAh g^{-1} tested at 600 mA g^{-1} after 50 cycles and good rate performance at room temperature. Compared with the pure SnO_2@C, SnO_2@C/Cu anodes exhibited obviously better low-temperature electrochemical performance including reversible capacity, cycling performance, and rate performance. In addition, new insights on the impedance analysis for enhanced mechanism are provided.

2. Experimental

2.1. Materials synthesis

All chemicals in this work were of analytical grade and used as received. In a typical experiment, 10 mmol sodium stannate (Na_2SnO_3) was dissolved in 50 ml of 1 M glucose aqueous solutions. The clear solution was obtained through ultrasonic dispersion for 1 h before being transferred to a Telflon-lined stainless steel autoclave heated at 180 °C for 4 h. The precipitates were harvested by centrifugation and washed thoroughly with deionized water and ethanol several times, respectively. After drying at 80 °C overnight, SnO_2 powders and SnO_2@C powders were obtained at 550 °C for 4 h with a heating rate of 2 °C min^{-1} under air and argon atmosphere, respectively. SnO_2@C/Cu sample was synthesized as follows. 250 mg SnO_2@C powders were dissolved in 100 ml 8 mM $CuSO_4$ aqueous solution through ultrasonic dispersion for 1 h. Afterward, 5 ml hydrazine hydrate ($N_2H_4{\cdot}H_2O$) was dripped into the solution slowly. SnO_2@C/Cu powders were harvested after centrifugation and dried at 80 °C under vacuum.

2.2. Materials Characterization

The samples were characterized by X-ray diffraction (XRD, RIGAKU SCXmini), scanning electron microscope (SEM, Hitachi SU8010), energy dispersive X-ray spectroscopy (EDS, Hitachi SU8010), transmission electron microscope (TEM, Tecnai G2 F20) and thermogravimetry analyses (TGA, NETZSCH STA449C).

2.3. Electrochemical measurements

The electrochemical behaviors were measured via CR2025 coin-type cells assembled in a dry argon-filled glove box. The test cell consisted of working electrode (about 1.2–1.5 mg cm^{-2}) and lithium sheet which were separated by a Celgard 2300 membrane and electrolyte of 1 M $LiPF_6$ in EC: EMC: DMC (1:1:1 in volume). The working electrode consisted of 80 *wt.%* active material, 10 *wt.%* acetylene black, and 10 *wt.%* polymer binder (Carboxymethylcellulose, Na-CMC). The electrodes were dried at 80 °C overnight in a vacuum. These electrochemical properties are all calculated based on the overall mass of the active material. The cells were cycled by LAND2001A at room temperature. Cyclic voltammetry curves (CVs) were tested on a CHI660D Electrochemical Workstation with a scan rate of 0.5 mV s^{-1}. Electrochemical impedance measurements were carried out by applying an ac voltage of 5 mV over the frequency from 1 mHz to 100 kHz.

3. Result and discussion

The crystalline structure of SnO_2@C and SnO_2@C/Cu has been characterized by XRD. Fig. 1 shows that the typical diffraction peaks at 2θ = 26.6, 33.9, 37.9, 51.8, 54.7, 57.8, 61.9, 64.7, 65.9, 71.3 and 78.7 degree presented in both of SnO_2@C/Cu and SnO_2@C are attributed to the reflections of (1 1 0), (1 0 1), (2 0 0), (2 1 1), (2 2 0), (0 0 2), (3 1 0), (1 1 2), (3 0 1), (2 0 2) and (3 2 1) planes of tetragonal SnO_2 structure (JCPDS no. 41-1445), respectively. Compared with SnO_2@C, SnO_2@C/Cu presents three additional clear diffraction peaks, being matched well with the (1 1 1), (2 0 0), (2 2 0) crystal planes of Cu (JCPDS no. 65-9743). Thus, it is suggested that Cu was successfully introduced into the composite, providing a good conductivity for the SnO_2@C/Cu. In addition, the broad peaks presented for SnO_2 and Cu indicated their nanocrystalline particles, which are in agreement with the following TEM results. Furthermore, as shown in the TGA result in Fig. S1, the loading ratio of SnO_2 in SnO_2@C and SnO_2@C/Cu composites were about 67 *wt.%* and 62 *wt.%*, and that of Cu and C in the SnO_2@C/Cu composite were about 7 *wt.%* and 31 *wt.%*, respectively.

The morphologies and sizes of SnO_2, SnO_2@C and SnO_2@C/Cu were characterized by SEM measurements. As shown in Fig. 2a and b, the bare SnO_2 products are uniform pomegranate-core-like nano-spheres with diameters of approximately 90–110 nm. It is also observed that the pomegranate-core-like SnO_2 nano-spheres are composed of many smaller nanoparticles with a diameter of ~8 nm. Meanwhile, Fig. 2c and d present the panoramic SEM images for the SnO_2@C composite, respectively. With the carbon coating, the entire SnO_2@C composite are composed of smooth

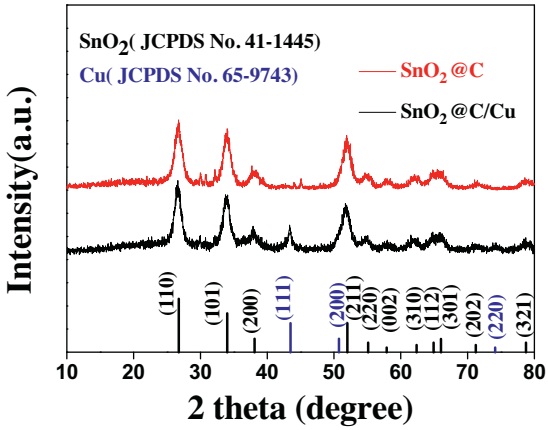

Fig. 1. XRD patterns of the SnO_2@C and SnO_2@C/Cu.

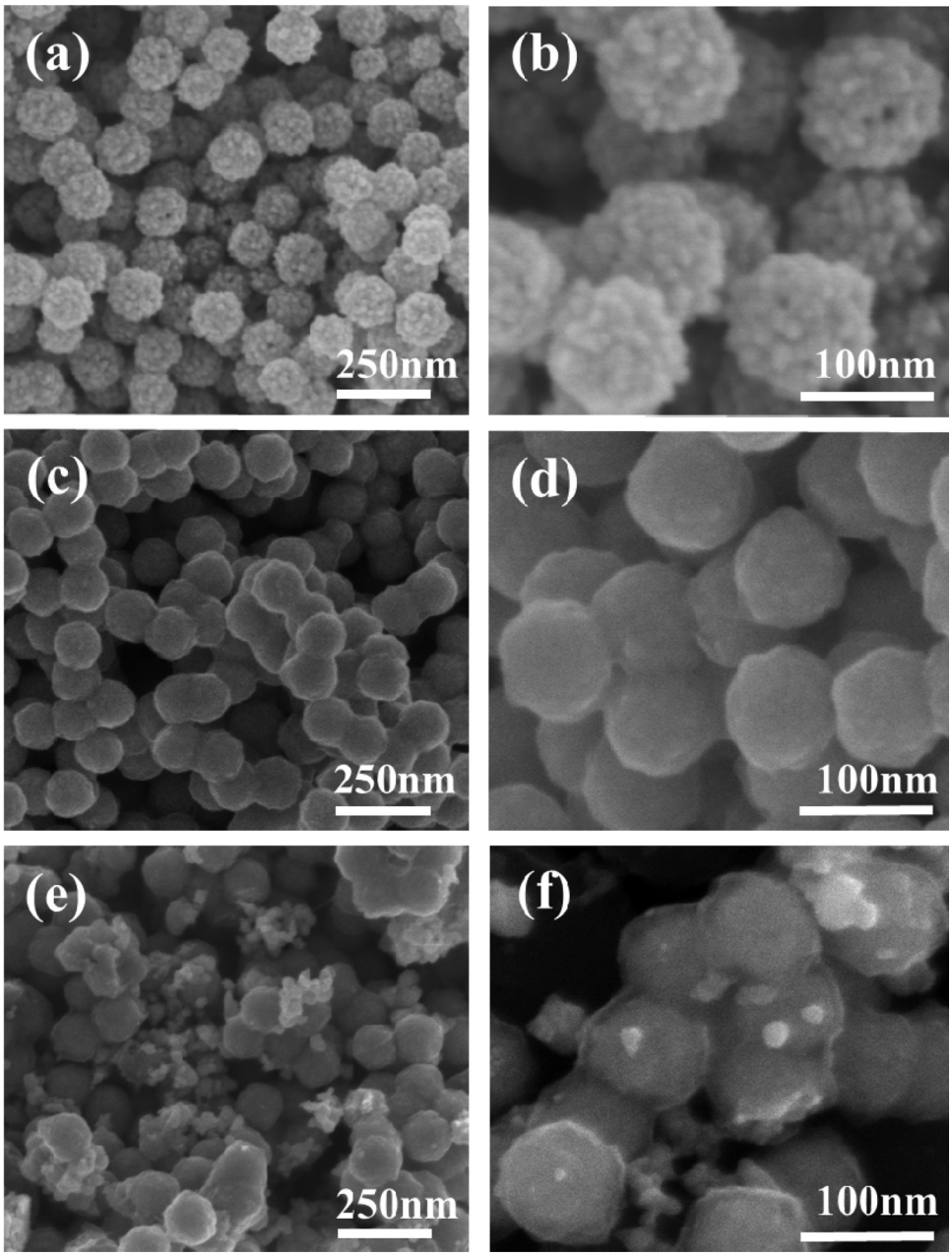

Fig. 2. SEM images of the (a,b) pure SnO_2, (c,d) SnO_2@C and (e,f) SnO_2@C/Cu.

ball-like NPs with the similar diameters in comparison of bare SnO_2. As further shown in the SEM images of Fig. 2e and f, the detailed morphologies and structure features of SnO_2@C/Cu are depicted. These SEM images clearly display that adding Cu particles does not change the general shape of SnO_2@C NPs but results in the difference in the surface morphology of the hybrid products. It is observed that massive Cu nanoparticles are attached on the surface and gap of SnO_2@C nano-spheres. The EDS result in Fig. S2 also supported the existence of Cu nanoparticles. These uniform Cu nanoparticles are beneficial to the fast diffusion and migration of electronics in the metal conductor especially at low temperature, thereby improving their electrochemical performance of electrodes. In order to further confirm the presence of Cu, element mapping was used to observe the distribution of each element. As presented in Fig. 3, the color points are due to the presence of the element. It can be seen that C, O, Sn and Cu in the sample are homogeneously distributed in the composite. Similarly, the Fig. S3 also indicated this phenomenon.

As we know, carbon shell has been demonstrated to offer residual buffer space to accommodate the large volume change and weaken secondary agglomeration of SnO_2 particles during cycling. TEM images of SnO_2@C and SnO_2@C/Cu were conducted to characterize their structure. Meanwhile, the TEM images of SnO_2 have been presented in Fig. S4 for comparison. From Fig. 4, almost all the samples are sphere-like and core-shell morphology. Hereinto, the element mapping test for SnO_2@C shown in Fig. S5 displayed that the C-shell and Sn-O-core are clearly distinguished. For SnO_2@C/Cu, the irregular Cu particles signed by arrow were also presented in the Fig. 4b. Furthermore, the insets of HR-TEM image shown in both of Fig. 4a and b revealed the interplanar spacing of 0.335 and 0.264 nm, corresponding to the (1 1 0) and (1 0 1) planes of SnO_2 in both samples. It is noted that the surface contact between C shells and the contact between C shells

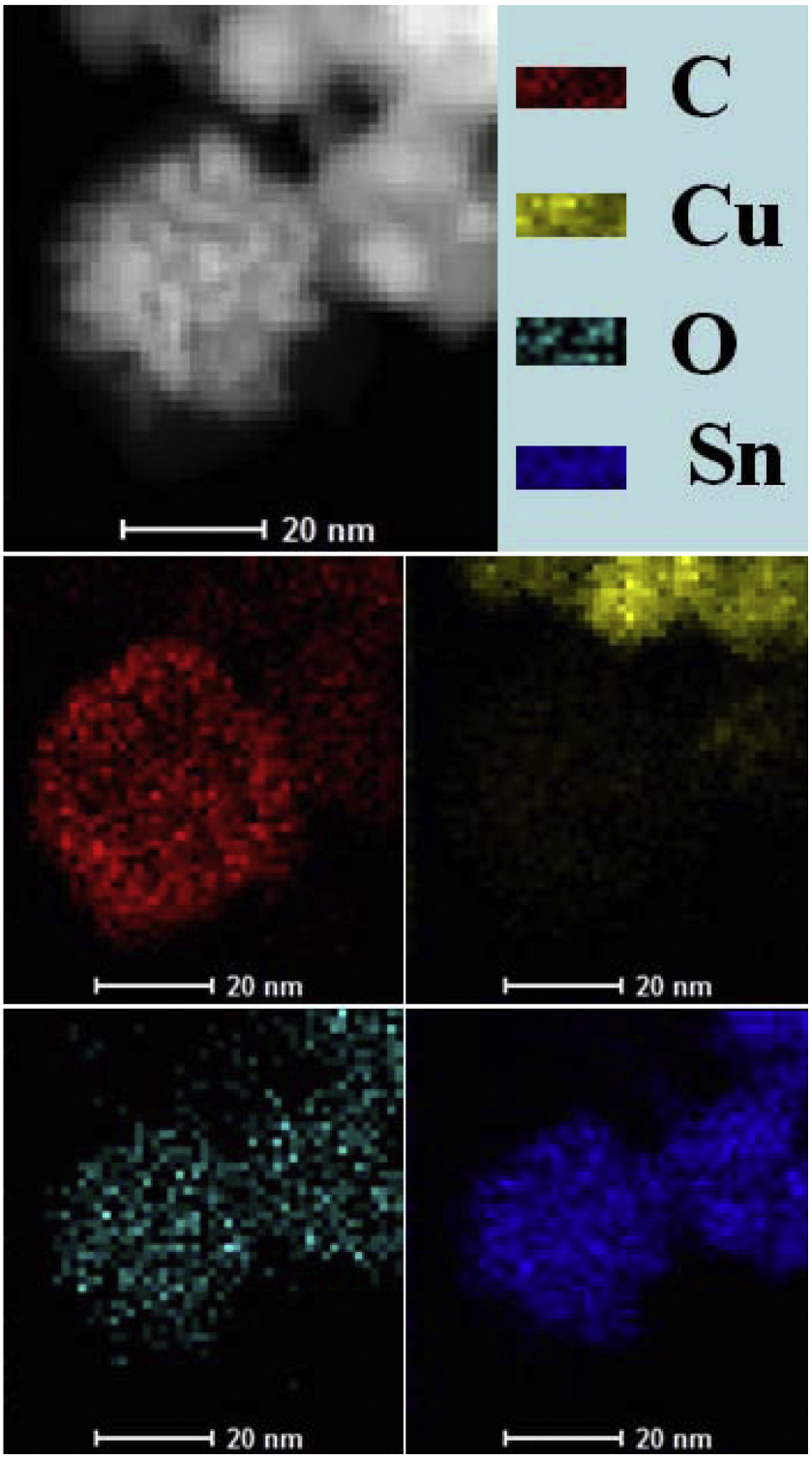

Fig. 3. STEM image and carbon, copper, oxygen, tin element mapping images of as-obtained SnO_2@C/Cu.

and Cu particles should be both considered to be beneficial to enhance electronic conductivity and improve electrochemical performance of their electrodes for LIBs.[21]

Cyclic voltammograms were performed to study the reaction mechanism of SnO_2@C and SnO_2@C/Cu electrodes. The cyclic voltammetry (CV) curves of SnO_2@C and SnO_2@C/Cu electrodes at first 5 cycles between 0.05 and 3 V at the rate of 0.5 mV s^{-1} are shown in Fig. 5a and b. Fig. S6a shows the initial six CVs of bare SnO_2 electrode for comparison. In the first cathodic scan, the sharp reduction peak at 0.75 V corresponds to the formation of solid electrolyte interface (SEI) layer and the reduction of SnO_2 to metallic Sn, as described in equations (1) and (2) [22–23]. The other broad peak extending to 0.05 V is ascribed to the formation of a series of Li-Sn alloy. After forming stable SEI layer at the first cycle, the following reduced reactions corresponding to equations (1) and (2) provided peaks at around 1.1 V. This result is similar to the related reports [17,23]. On the contrary, the oxidation peak at 0.62 V in the anodic scan indicates the highly reversible de-alloying

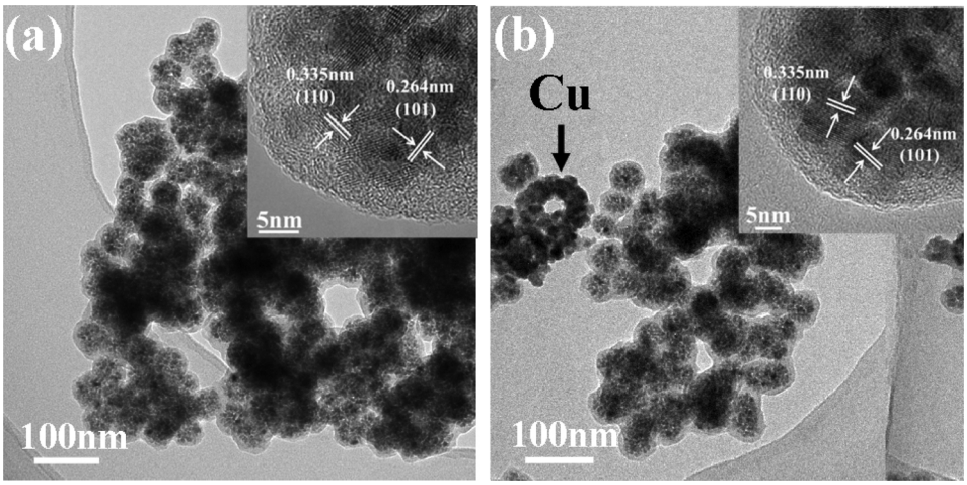

Fig. 4. TEM and the corresponding HR-TEM images of the (a,b)SnO_2@C and (c,d)SnO_2@C/Cu.

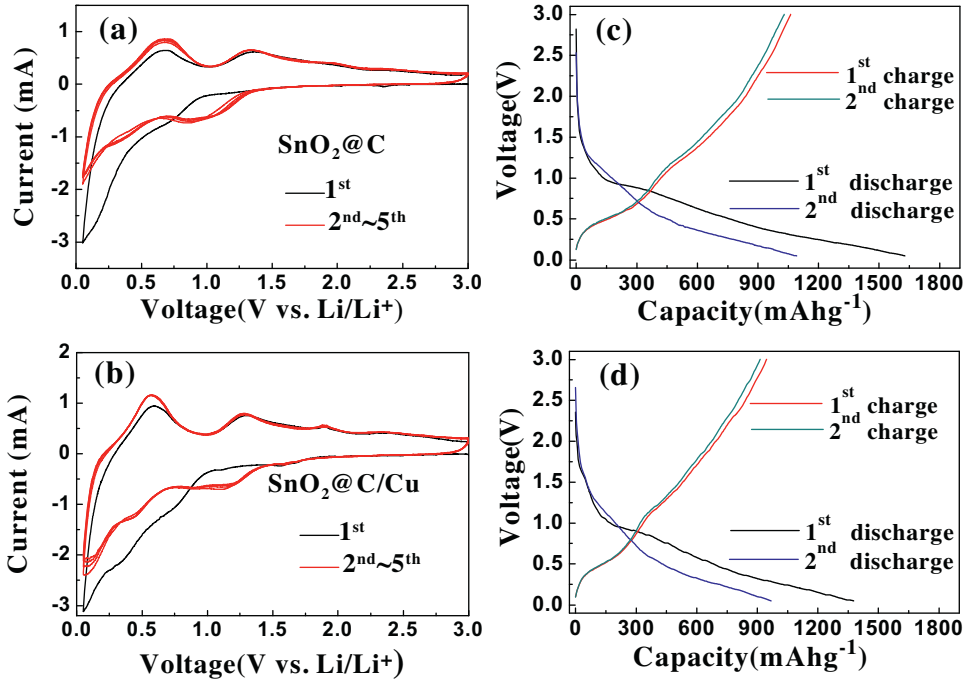

Fig. 5. Cyclic voltammetry curves and first two discharge-charge curves between 0.05 and 3 V of Li insertion/extraction into/from two electrodes: (a, c) SnO_2@C electrode and (b, d) SnO_2@C/Cu electrode.

of Li_xSn as pointed out by equation (3). The following peak at 1.25 V is ascribed to the partially reversible reaction in equation (2). Compared with the bare SnO_2 electrode, both of CVs for SnO_2@C and SnO_2@C/Cu electrodes shown in Fig. 5a and b presented that the peaks extending from 1.0 V to 0.05 V are obvious broaden than that of SnO_2 electrode, indicating the Li^+ insertion into carbon shell. The related redox mechanism for other peaks presented in CVs is consistent with that of SnO_2 electrode as above-mentioned. However, both of CVs for SnO_2@C and SnO_2@C/Cu electrodes display a different electrochemical behavior compared to the bare SnO_2 electrode. The redox peaks of the following cycles are very close to the 1st one, which exhibits good reproducibility and similar shapes, revealing better electrochemical stability for SnO_2@C and SnO_2@C/Cu anodes. This phenomenon can relieve the aggregation and pulverization of SnO_2 nanoparticles during the discharge/charge process, suggesting only little capacity loss in the following cycles.

$$Li^+ + 4e^- + \text{electrolyte} \rightarrow Sn + 2Li_2O \quad (1)$$

$$SnO_2 + 4Li^+ + 4e^- \rightarrow Sn + 2Li_2O \quad (2)$$

$$Sn + xLi^+ + xe^- \leftrightarrow Li_xSn\ (0 \le x \le 4.4) \quad (3)$$

Accordingly, the discharge/charge (D/C) profiles of the SnO_2@C and SnO_2@C/Cu electrodes in the first two cycles at a current density of 200 mA g^{-1} between 0.05 V and 3.00 V are presented in Fig. 5c and d, respectively. The first two D/C profiles for SnO_2 electrode were also shown in Fig. S6b. Those voltage plateaus shown in D/C profiles for the SnO_2, SnO_2@C and SnO_2@C/Cu

electrodes are consistent with the CVs observation. It is found that the first coulombic efficiency for SnO_2, SnO_2@C and SnO_2@C/Cu are about ~58 % (i.e., 1060/1760), ~63 % (i.e., 1040 /1650) and ~66 % (i.e., 960 /1375), respectively. The improvement for the first coulombic efficiency should benefit from the carbon coating and Cu particles. In addition, the lower initial discharged capacity for SnO_2@C/Cu is obtained, which may be resulted from the additional weight of Cu element in SnO_2@C/Cu composites.In other words, this large capacity loss in the first cycle corresponded to the formation of the SEI layer, which was consistent with the CV observation.

Fig. 6 and S7 compared the cycling performance of SnO_2, SnO_2@C and SnO_2@C/Cu electrodes. The SnO_2@C anode exhibits much better cyclic stability than that of bare SnO_2 anode with reversible capacity of SnO_2 only remained at ~50 mAh g^{-1} after 50 cycles. The quick capacity fading of bare SnO_2 should be resulted from severe aggregation and pulverization of SnO_2 nanoparticles in the charge and discharge processes. Importantly, the LIB performance for SnO_2@C anode can be further enhanced by introducing metal Cu particles. It is observed from Fig. 6a that the reversible capacity of SnO_2@C/Cu can remain at ~740 mAh g^{-1} tested at 200 mA g^{-1} after 60 cycles, being larger than that of only 450 mAh g^{-1} for the SnO_2@C anode. Similarly, the SnO_2@C and SnO_2@C/Cu electrodes were cycled under a relatively high current density of 600 mA g^{-1} after being activated at 200 mA g^{-1} in the first three cycles. As displayed in Fig. 6b, the specific capacity and cycling performance of the SnO_2@C/Cu composite was improved by adding Cu particles compared with SnO_2@C electrode. The improved electrochemical performance for the SnO_2@C/Cu electrodes can be attributed to the adding of the Cu particles, which may contribute positively to the conductance and SnO_2@C stabilization. According to the EIS result shown in Fig. S8, the good performance of SnO_2@C/Cu electrodes is also ascribed to the good conductivity and electronic contact between SnO_2@C and Cu particles.

In addition to good electrochemical stability of SnO_2@C/Cu electrodes, the rate performance was tested by changing the current density. As presented in Fig. 6c, the stable capacities at different current densities can be observed, even at a high rate of 1000 mA g^{-1}. The reversible capacity of SnO_2@C/Cu remained at ~650 mAh g^{-1} tested at 200 mA g^{-1} after 55 cycles. It is observed that the obtained LIB rate performance for SnO_2@C/Cu was much better than that of SnO_2@C electrode. The Cu NPs possess good conductivity for their anodes, thereby significantly improving the electrochemical performance for their composites. As displayed in the following Fig. S9, the good morphology retention after electrochemical testing for pomegranate-structured SnO_2@C/Cu can be obtained. However, without the protection of C shell, the Fig. 1a and b revealed that the pure SnO_2 electrode cannot prevent pulverization and maintain initial pomegranate-structured morphology. Furthermore, Fig. S10 shows the TEM and HR-TEM images for SnO_2@C/Cu after cycling. The good morphology retention after electrochemical testing can effectively facilitate the high stability for the electrochemical performance of the SnO_2@C/Cu electrodes.

With copper being a better conductor than carbonaceous material, introducing Cu particles into the SnO_2@C/Cu composites can enhance their LIB performance especially at low temperature. Fig. 7 shows the cycling performance at 600 mA g^{-1} and rate performance at different current densities for the SnO_2@C and SnO_2@C/Cu electrodes under low temperatures of 5 °C, respectively. Hereinto, the first two D/C profiles for these two electrodes were also shown in Fig. S11. Importantly, the SnO_2@C/Cu electrode exhibited good cycling performance at a high current density of 600 mA g^{-1}, as shown in Fig. 7. After 60 discharge/charge cycles,

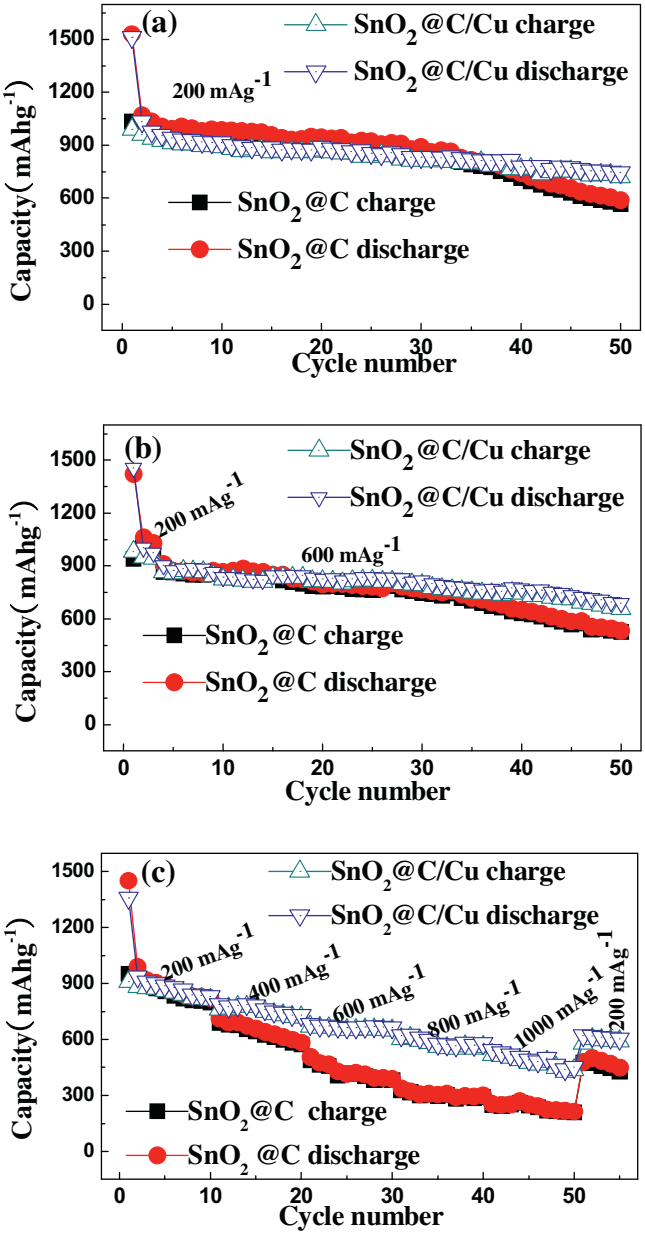

Fig. 6. Cycling performance of SnO_2@C and SnO_2@C/Cu electrodes at room temperature: (a) at a current density of 200 mA g^{-1}; (b) at a large current density of 600 mA g^{-1}; (c) rate cycling performance.

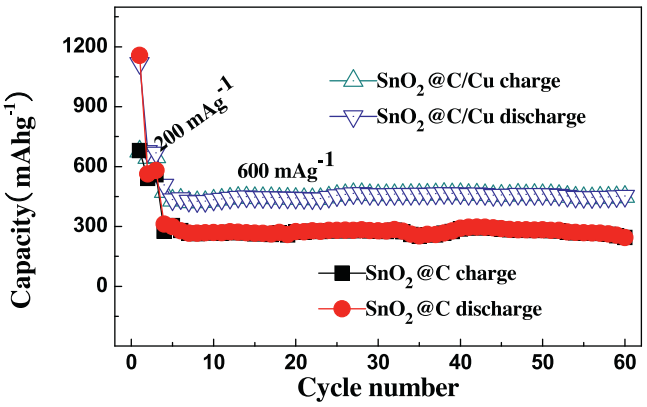

Fig. 7. Cycling performance of SnO_2@C and SnO_2@C/Cu electrodes at the low temperature of 5 °C: (a) at a current density of 600 mA g^{-1}.

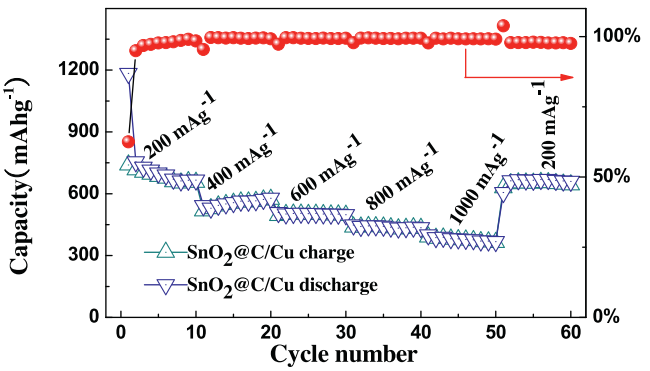

Fig. 8. Rate cycling performance of SnO_2@C and SnO_2@C/Cu electrodes at the low temperature of 5 °C.

the SnO_2@C/Cu electrode still delivered reversible charge capacities of 420 mA h g^{-1}, which is much larger than that of 240 mA h g^{-1} for SnO_2@C electrode. Meanwhile, it is expected that the SnO_2@C/Cu anode exhibit much better rate performance with cyclic stability than the SnO_2@C anode as shown in Fig. 8. When the current density is turned back to 200 mA g^{-1} after 60 cycles at various rates, the capacity for SnO_2@C/Cu can recover to 630 mAh g^{-1}. It is also observed that the obtained LIB coulombic efficiency for SnO_2@C/Cu was about 99%.

Figs. S12 and 13 presented electrochemical impedance spectroscopy (EIS) of SnO_2@C and SnO_2@C/Cu electrodes after test and the corresponding equivalent circuits. According to the literature [24], the high-frequency semicircle is related to Li ion migration through the SEI film covering the surface of the electrode, the middle-frequency semicircle is attributed to charge transfer through the electrode/electrolyte interface, and the steep sloping line is assigned to solid-state diffusion of the Li ions into the bulk of the electrode material. The impedance spectra are fitted with an equivalent circuit as shown in the insets of Figs. S12 and 13, where the symbols, R_e,R_{sf}, R_{ct}, and R_w, denote the solution resistance, the diffusion resistance of Li ions through SEI layer, the charge-transfer resistance and Warburg impedance, respectively. Tables S1 and S2 indicated that the difference of total resistance between SnO_2@C and SnO_2@C/Cu electrodes tested at room temperature are about three hundreds of Ohm. Most importantly, this difference

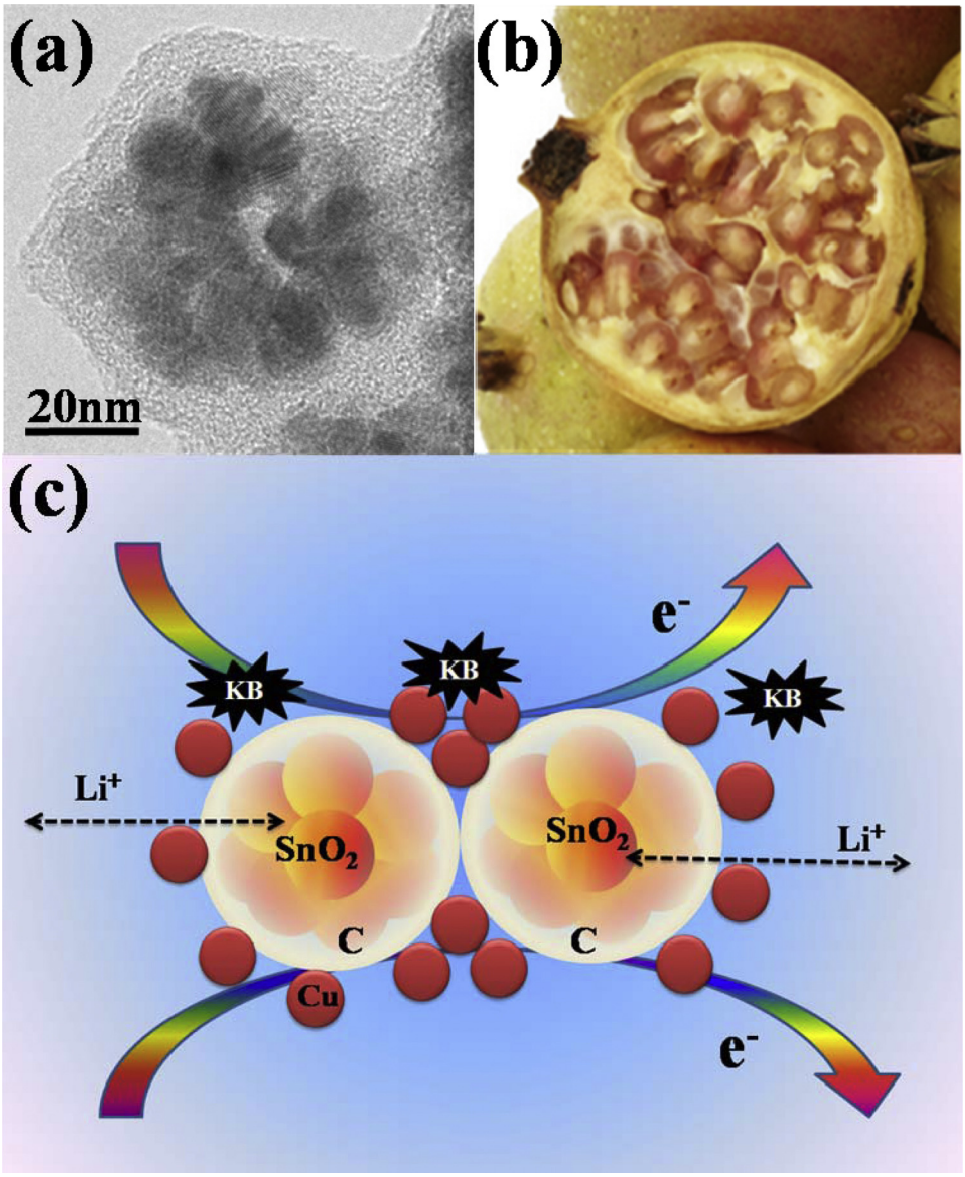

Fig. 9. (a) the TEM image of solo pomegranate-structured SnO_2@C composite, (b) the photo of pomegranate, (c) the phenomenological resistance model.

increased sharply to about one thousand of Ohm when the temperature was reduced to 5 °C, demonstrating a more deteriorated resistance for pure carbon coating tested at a lower temperature. Thus, the improved performance should be caused by the enhanced conductivity and unique architecture of SnO_2@C/Cu.

As revealed in Fig. 9, for SnO_2 anodes, using carbon shell coating coupled with the adding Cu particles to form homogeneous composites of pomegranate-structured SnO_2@C/Cu, and further to prevent the agglomeration of active materials and the capacity fading in cycling process, is promising for high-performance LIBs especially at low temperature. Moreover, the LIBs in practical application were usually carried out under direct-current mode. As presented in Fig. 9c, according to scattering theory of electron transport across the interface, the total resistance of SnO_2@C/Cu in batteries is determined by the resistance of Cu particles, which is much smaller than the carbon shell in the composites of SnO_2@C. Thus, the improvement of conductivity in electrode can result in a low interface polarization, which is considered to be responsible for the enhancement of the electrochemical performance.

4. Conclusion

Composites of Cu particles decorated pomegranate-structured SnO_2@C (SnO_2@C/Cu) have been prepared by a simple hydrothermal reaction coupled with wet-chemical reduction and used as anodes for LIBs. The SnO_2@C/Cu anodes can exhibit good lithium battery performance with a capacity of 660 mAh g^{-1} tested at 600 mA g^{-1} after 50 cycles and good rate performance at room temperature. Compared with the pure SnO_2@C, the SnO_2@C/Cu anodes exhibited obviously better low-temperature electrochemical performance including reversible capacity, cycling performance, and rate performance. These enhanced LIB properties for SnO_2@C/Cu should be contributed from the synergistic effect of the pomegranate-like structure and the conducting Cu particles decorating.

Supporting information

SEM and TEM images, SAED Raman and EDS patterns, CV curves, discharge curves, and Electrochemical impedance spectra. This materials are available free of charge *via* the Internet.

Acknowledgment

We acknowledge the financial support by National Fundamental Research Program of China (Grant No.2011CBA00200), the Natural Science Foundations of China (No.21203025), Fund of Education Committee of Fujian Province (JK 2013010 and JA13064), Science and technology major projects of Fujian Province (2013HZ0003) and project of Fujian Development and Reform Commission (2013-577).

Appendix A. Supplementary data

Supplementary data associated with this article can be found, in the online version, at http://dx.doi.org/10.1016/j.electacta.2015.09.082.

References

[1] L. Lu, X. Han, J. Li, J. Hua, M. Ouyang, Journal of Power Sources 226 (2013) 272–288.
[2] J.S. Chen, X.W. Lou, Small 9 (2013) 1877–1893.
[3] Y. Dong, Z. Zhao, Z. Wang, Y. Liu, X. Wang, J. Qiu, ACS applied materials & interfaces 7 (2015) 2444–2451.
[4] C. Wang, G. Du, K. Ståhl, H. Huang, Y. Zhong, J.Z. Jiang, The Journal of Physical Chemistry C 116 (2012) 4000–4011.
[5] J. Li, W. Wen, G. Xu, M. Zou, Z. Huang, L. Guan, Electrochimica Acta 153 (2015) 300–305.
[6] X. Xu, J. Liang, H. Zhou, D. Lv, F. Liang, Z. Yang, S. Ding, D. Yu, Journal of Materials Chemistry A 1 (2013) 2995.
[7] Y. Zhu, H. Guo, H. Zhai, C. Cao, ACS applied materials & interfaces 7 (2015) 2745–2753.
[8] J. Zhu, J. Jiang, Y. Feng, G. Meng, H. Ding, X. Huang, ACS applied materials & interfaces 5 (2013) 2634–2640.
[9] W. Chen, D. Deng, Carbon 87 (2015) 70–77.
[10] L. Li, A. Kovalchuk, J.M. Tour, Nano Research 7 (2014) 1319–1326.
[11] C. Guan, X. Wang, Q. Zhang, Z. Fan, H. Zhang, H.J. Fan, Nano letters 14 (2014) 4852–4858.
[12] Z. Wen, F. Zheng, K. Liu, Materials Letters 68 (2012) 469–471.
[13] X. Liu, X. Zhong, Z. Yang, F. Pan, L. Gu, Y. Yu, Electrochimica Acta 152 (2015) 178–186.
[14] M.O. Guler, O. Cevher, T. Cetinkaya, U. Tocoglu, H. Akbulut, International Journal of Energy Research 38 (2014) 487–498.
[15] J.H. Um, S.-H. Yu, Y.-H. Cho, Y.-E. Sung, New Journal of Chemistry (2015) 392541–392546.
[16] Y. Wang, Z.X. Huang, Y. Shi, J.I. Wong, M. Ding, H.Y. Yang, Scientific reports 5 (2015) 9164.
[17] Y. Zhao, J. Li, N. Wang, C. Wu, G. Dong, L. Guan, The Journal of Physical Chemistry C 116 (2012) 18612–18617.
[18] M. Zou, J. Li, W. Wen, L. Chen, L. Guan, H. Lai, Z. Huang, Journal of Power Sources 270 (2014) 468–474.
[19] N. Liu, Z. Lu, J. Zhao, M.T. McDowell, H.W. Lee, W. Zhao, Y. Cui, Nature nanotechnology 9 (2014) 187–192.
[20] X. Zhou, W. Liu, X. Yu, Y. Liu, Y. Fang, S. Klankowski, Y. Yang, J.E. Brown, J. Li, ACS applied materials & interfaces 6 (2014) 7434–7443.
[21] J. Deng, C. Yan, L. Yang, S. Baunack, S. Oswald, H. Wendrock, Y. Mei, O.G. Schmidt, Acs Nano 7 (2013) 6948–6954.
[22] J. Li, M. Zou, Y. Zhao, Z. Huang, L. Guan, RSC Advances 3 (2013) 19251.
[23] J. Li, Y. Zhao, N. Wang, L. Guan, Chem Commun (Camb) 47 (2011) 5238–5240.
[24] J. Li, M. Zou, Y. Zhao, Y. Lin, H. Lai, L. Guan, Z. Huang, Electrochimica Acta 111 (2013) 165–171.